Blackebergs gymnasium
Naturvetenskap inr. Naturvetenskap
Gymnasiearbete 100p
HT 2018 – VT 2019

Quantifying Asymmetries in Supernovae

A Study on the Deaths of Massive Stars

Miranda Jäderling
miranda.jaderling@gmail.com
Supervisor: Dennis Alp, KTH

BLACKEBERGS GYMNASIUM

Contents

Abstract

Supernovae are among the most energetic phenomena in the cosmos, occurring at the end of the life of a massive star. The stellar explosions not only supply the universe with kinetic energy, but they also fuel chemical reactions and the creation of elements, as well as provide the material and conditions required for new stars and planets to form. Neutron stars and black holes are also results of these explosions. In order to study the many intricate processes in supernovae, astrophysicists use numerical computer simulations in addition to observational data. These simulations give an insight to the asymmetries in supernovae, which are thought to play a crucial role in the origin and mechanisms of the supernova explosion. In this study, the programming language Python has been used to quantify geometrical properties in these numerical simulation models. The results suggest that rotation in the supernova is what possibly causes the elements to be expelled in a coplanar manner. The results also show that the heavier elements, i.e. the core elements in the progenitor star, have centres of mass with the highest velocities in the supernova ejecta, and that the supernovae are more asymmetric in the intermediate than in the innermost regions of the ejecta. In this paper, a method of presenting and defining asymmetries in supernovae using the centre of mass for the different elements in the ejecta is also proposed.

List of abbreviations

Listed alphabetically.

BSG	blue supergiant
CoM	centre of mass
H-R diagram	Hertzsprung-Russell diagram
$M_\odot$	solar mass, the mass of our sun = 1.9891×10^{33} g
NS	neutron star
RSG	red supergiant
RT instability	Rayleigh-Taylor instability
SN/SNe	supernova/supernovae
SNR	supernova remnant

1. Introduction

Supernova (SN, core-collapse unless stated otherwise) explosions are huge explosions in space caused by massive stars (mass > 8 $M_{\odot}$) dying. The SN can reach a maximum luminosity equal to the total luminosity of an entire galaxy, and the explosion expels large parts of the initial star into space at velocities of up to approximately 20 000 km/s. There are two main types of supernovae (SNe), type I and type II, which are defined by their light curves and absorption lines on their spectra. Usually, these explosions occur in distant galaxies. Very few SNe have been detected in our galactic neighbourhood in the last thousand years; the most recent being SN 1987A in the Large Magellanic Cloud, a satellite galaxy to the Milky Way about 179 000 light years away, in 1987 (NASA, 2015)(NE, 1996). In this study the asymmetric properties of SNe, which are thought to be an important proxy of the SN explosion mechanism, are examined.

1.1 Stars

In order to understand the mechanisms of SNe, one must first understand the type of stars from which they originate. Stars are huge spherical celestial bodies of gas that consist mostly of hydrogen. They are created within nebulae, which are giant clouds of gas and dust. Irregularities in these clouds cause turbulence, which in turn causes more massive parts of the cloud to collapse under its own gravitational attraction. Due to the collapse, the gas and dust starts to heat up. More material is attracted from the surrounding nebula, creating a hot and dense protostar. If the mass of the protostar is less than 0.08 $M_{\odot}$ it does not ignite and instead becomes a brown dwarf, but if its mass exceeds this limit the protostar eventually becomes sufficiently hot to fuse hydrogen atoms into helium. This thermonuclear reaction creates an outward pressure that balances the inward force of gravity, thus stabilizing the star (NASA, 2018) (Taylor Redd, 2018).

Figure 1 shows a Hertzsprung-Russell (H-R) diagram, which describes the evolutionary sequence of stars, and includes almost all stages in the life of a star. Stars with a stable thermonuclear process are called main sequence stars, and occupy the diagonal band in the graph in *Figure 1*. Approximately 90% of all stars are main sequence stars (Smithsonian Astrophysical Observatory, 2017). Stars to the right in the diagram have lower surface temperatures, while stars to the left have higher surface temperatures. The location of a star on the main sequence band is determined by its mass. Stars to the upper left on the main sequence are more massive and luminous than our sun while stars to the lower right are less massive and dimmer (this relationship between mass and luminosity is only true for stars on the main sequence band).

As main sequence stars run out of hydrogen, the outward pressure decreases, and the star moves through a series of evolutionary stages; the exact stages depend on their initial mass (Smithsonian Astrophysical Observatory, 2017). E.g. our sun is currently a main sequence star (as can be seen in *Figure 1*), but when its hydrogen is depleted, its core will increase in temperature and density. The outer layers will expand; resulting in the sun becoming a red giant; seen on the giants-branch of the H-R diagram. It will then go through stages of hydrogen and helium fusion until it sheds approximately half of its mass to form a planetary nebula, the remnant being a white dwarf (located to the lower left in the H-R diagram) (Wikipedia, 2018). Main sequence stars with masses between ~ 0.08 $M_{\odot}$ and 8 $M_{\odot}$ go through similar stages, the more massive ones fusing elements up to carbon before turning into white dwarves (Smithsonian Astrophysical Observatory, 2017). The white dwarves are extremely hot and dense, a typical white dwarf has a mass of 0.7 $M_{\odot}$, a radius of approximately 8 000 km, and a surface temperature of 10 000 K (NE, 1996). The surface temperature of a white dwarf can be between 4 000 K and 100 000 K, but the mass always is lower than ~ 1.4 $M_{\odot}$, the so-called Chandrasekhar limit. If the mass of a white dwarf exceeds this critical limit, nuclear reactions are triggered with such a speed that the white dwarf explodes in a thermonuclear SN (see section *1.2*).

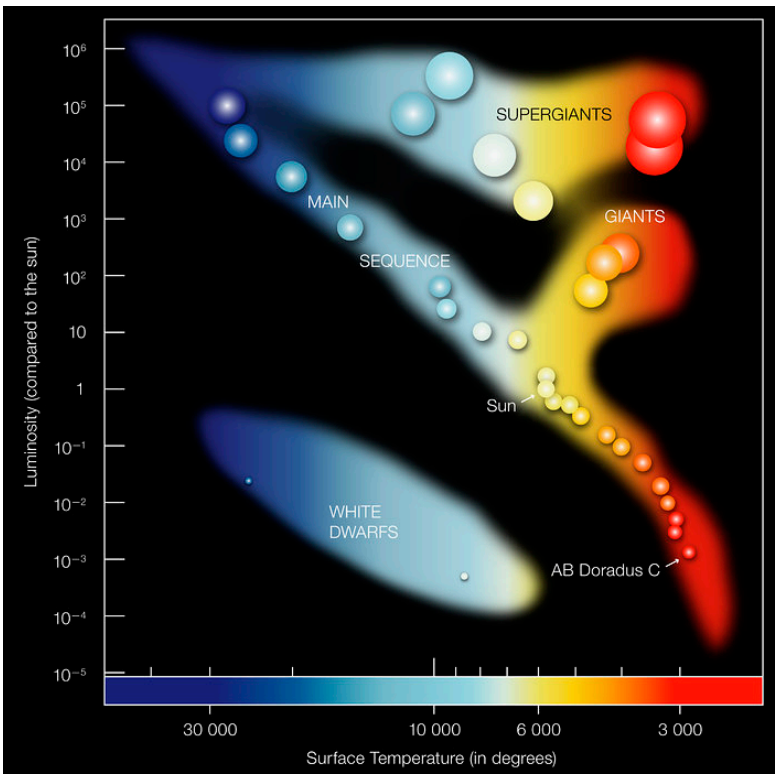

Figure 1. Hertzsprung-Russell diagram.

(ESO. 2007. *Hertzsprung-Russell diagram*. Available from: https://www.eso.org/public/usa/images/eso0728c/. (CC BY 4.0) https://creativecommons.org/licenses/by/4.0/ [2018-12-25])

Stars with mass above ~ 8 $M_{\odot}$ are massive enough to move onto the supergiant-branch after hydrogen depletion, gradually expanding into cool and extremely luminous red supergiants. These are the type of stars that ultimately become core-collapse SNe. In these massive stars, the core pressure and temperature eventually becomes great enough to allow fusion of heavier elements than in the giants, creating neon, magnesium, silicon and sulphur (Smithsonian Astrophysical Observatory, 2017). These elements continue to fuse until iron, nickel, and other elements of similar atomic weight are created. Iron- and nickel fusions are endothermic reactions, meaning that energy is not released as it is during fusion of lighter elements. Because of this, fusion of iron and nickel does not occur naturally and an inert core of iron and nickel is created in the centre of the star. *Figure 2* shows the layering of elements in massive stars directly after creation of iron and nickel. The nucleosynthesis, the fusion of elements, takes place on the borders between layers. As the fusion of elements in the core stops, the outward nuclear force balancing the inward pressure of gravity decreases, and the supergiant collapses into a core-collapse SN (see section *1.2*).

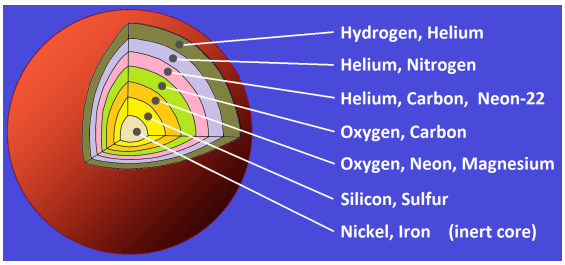

Figure 2. Diagram showing the layering of elements in a massive star pre-collapse.
(FT2. 2011. *Massive star cutaway pre-collapse*. Available from: https://commons.wikimedia.org/wiki/File:Massive_star_cutaway_pre-collapse_(pinned).png. (CC0 1.0) https://creativecommons.org/publicdomain/zero/1.0/deed.en [2018-09-24])

1.2 Supernovae

There are two main types of SNe; Type I and Type II. SNe were originally classified by, among other optical properties, the absorption lines in their spectra; which show which elements are present in the SN. This resulted in the two main types, where SNe of Type II show evidence of hydrogen in the ejected material while SNe of Type I do not. Later research shows that there is another way of classifying SNe: by the type of star that became the SN. Type II, Ib and Ic all originate from massive progenitor stars with an inert core that collapses under its own gravity; these are called core-collapse SNe. Type Ia SNe are results of a thermonuclear explosion of a white dwarf. In this study only core-collapse SNe are included;

therefore, the properties of Type Ia SNe will not be explained further. Type Ib and Ic show a lack of hydrogen in their emission lines, as does the Type Ia, and they were thus originally classified together as Type I SNe. The absence of hydrogen is due to the fact that Type Ib and Ic SNe shed most of their hydrogen shell in an earlier stage and thus do not show any hydrogen in the ejected material of the SN (Smithsonian Astrophysical Observatory, 2013). The majority of Type II SNe originate from red supergiants (RSG), creating Type II-L (linear) or Type II-P (plateau) SNe. These two subtypes are defined by the light curves of the SNe, where Type II-L SNe show a linear decline in luminosity after the peak in brightness, while Type II-P SNe show a flat stretch during the decline. After SN 1987A it was discovered that blue supergiants (BSG) can also result in SNe of Type II; although, these SNe have slightly peculiar properties, such as a more slow-rising light curve (Filippenko, 2011). SNe of Type IIb are core-collapse SNe that initially show weak lines of hydrogen in their spectra, but which in later observations become undetectable. Type IIb SNe are the results of massive stars that have shed most of its hydrogen in an earlier stage, or a star with a binary companion that has attracted the hydrogen from the star (Wikipedia, 2018). There are several additional subtypes that will not be explained further in this paper, as they are not relevant to these studies.

Core-collapse SNe begin as stars with a mass > 8 $M_{\odot}$ that eventually fuse heavy elements into iron and nickel, forming an inert core. This core is under extreme gravitational pressure, and because no nuclear fusion occurs in the core, it is supported only by electron degeneracy pressure; a quantum mechanical phenomenon. When the mass of the inert core exceeds 1.4 $M_{\odot}$ the degeneracy pressure can no longer support the force of gravity, the core collapses and falls in on itself until a neutron star is formed. The collapse then ceases, which creates a shock wave that starts a process that ejects the outer layers of the star into space (Clark, 1997). After the explosion a supernova remnant (SNR), consisting of the ejected material, and a compact remnant are left behind. If the initial mass of the progenitor star, the so called zero-age main-sequence mass, is less than 20 $M_{\odot}$, the pressure and heat of the core-collapse causes protons and electrons to combine; forming an extremely dense sphere of neutrons, a neutron star. If the zero-age main-sequence mass is more than 20 $M_{\odot}$, the stellar core keeps collapsing into itself; forming a black hole with an infinite density that prevents everything in its proximity from escaping, even light.

1.3 Asymmetries in Supernovae

Observations of SN 1987A gave rise to the theory that SN ejecta are asymmetric, which is thought to play a crucial role in the explosion mechanisms and formation of the SN (Wollaeger et al. 2017). Early

evidence of asymmetry can be seen in the instabilities that occur in the SN ejecta after bounce. In the area directly above the newly formed neutron star (NS) convective instabilities cause early asymmetries behind the shock wave (Wollaeger et al. 2017, Wongwathanarat et al. 2015), while the interfaces of the carbon+oxygen layer, helium layer and hydrogen layer are especially prone to Rayleigh-Taylor (RT) instabilities (Hammer et al. 2010). This is a type of hydrodynamic instability of the interface between two fluids of different densities where the lighter fluid is pushing the heavier fluid (Sharp, 1983). RT instabilities are the primary cause of the fingering asymmetry that can be observed in SNe, which arises when expanding gas in the core is pushed outward through the outer layers of the progenitor star, destroying the onion shell structure. The RT instabilities are thought to be seeded by the asymmetries in the innermost layers of the ejecta during the first seconds of the explosion (Wongwathanarat et al., 2015).

Another process discussed in this study is the decay of ^{56}Ni. ^{56}Ni is an unstable isotope of nickel, meaning that it decays into ^{56}Co with a half-life of approximately 6 days. ^{56}Co later decays into ^{56}Fe with a half-life of 77 days (Nadyozhin 1994). This explains several aspects of the received results, as described further on in this paper.

1.4 Aims

Supernovae are one of the few processes that supply our universe with kinetic energy. They also fuel chemical reactions and the creation of elements. From the material expelled by the explosion, stars and planets are born, and core collapse SNe result in the creation of black holes or neutron stars. The fact that SNe are such complex and important processes in space makes them very interesting to study. The exact explosion mechanism of SNe is still not entirely known, and because the asymmetric properties of the ejecta are an important proxy for this, the asymmetries are closely studied.

One way to study SNe is by creating computer simulations of collapsing stars and comparing the resulting models with actual observations. These computed numerical models can be used to describe asymmetries in the SN ejecta and attempt to explain the asymmetries we observe in real-life SNe. As of today there are no exact properties universally used to measure asymmetries in SNe, vague terms such as “plumes” or “fingers” are often used to define the asymmetry of a SN, which makes comparison of different SNe and SN models difficult. A generally accepted rule of description is therefore needed, such as presenting the centre of mass for each studied element in km s^{-1} instead of using terms such as “highly asymmetric” or “fast fingers”.

The aim of the present study was to propose a clearer definition of asymmetries in supernova remnants, as well as to study different geometrical properties in the SN. I have quantified geometrical properties such as the centre of mass for different elements in the ejected material and compared these with each other and with the neutron star created in the explosion. I have also studied the density of the different elements in the different layers of the SN and compared these with each other.

2. Methods

2.1 Models

In order to quantify the geometrical properties of SNe, I have used the programming language Python to study three-dimensional SN explosion models created and described by Wongwathanarat et al. (2015) and Menon et al. (2019). I have used the raw data received from these numerical simulations to calculate the centre of mass for the different elements in the supernova as well as to study the correlation of densities of different elements. These hydrodynamic simulations describe the explosion of core-collapse SNe from the moment the shock wave is initiated. In this study I have considered six different models of different progenitor stars: models B15-1, N20-4, L15-1, W15-2, W15-2-IIb (notation of Wongwathanarat, 2015) and 16-7b (notation of Menon et al. 2018), see *Table 1*. The models will from this point forward be referred to by the names of their respective progenitor star, see *Table 1*, where the two-digit number refers to the initial mass of the progenitor expressed in solar masses ($M_{\odot}$), and the letter is related to the creators of the models and does not correspond to any physical qualities.

Progenitor stars B15 and N20 are blue supergiants (BSG) designed to match the initial properties of SN 1987A, although these models are based on single-star progenitors while the SN 1987A could be the result of a binary merger progenitor. Model M15 is also designed to match the SN 1987A, but the progenitor star in this model is the result of a merger between a 16 $M_{\odot}$ primary and a 7 $M_{\odot}$ secondary star. Note that the mass of N20 is reduced from 20 $M_{\odot}$ to 16.3 $M_{\odot}$ at core-collapse due to mass loss. Progenitors L15 and W15 are red supergiants (RSG). Model IIb is created through removing all but the innermost 0.5 $M_{\odot}$ of the hydrogen envelope from the progenitor in model W15, thus allowing the star to explode as the SN Cassiopeia A, which was a Type IIb SN. In the version that I have used the models describe the SNe approximately 150 days after bounce for the non-stripped single progenitor models, i.e.

B15, N20, L15 and W15. Model IIb is developed until 18 days after bounce and model M15 until approximately 1.05 hours after bounce (see *Table 1*).

Table 1. SN explosion models used in this study. M_{NS} is the mass of the neutron star, M_{ej} is the mass of the SN ejecta, M_{tot} is the total mass at the time of the explosion and t_{late} is the time until which the model is developed. (Alp et al. 2018, Menon et al. 2019, Wongwathanarat et al. 2015)

Model	**Name**	**Type**	M_{NS} ($M_\odot$)	M_{ej} ($M_\odot$)	M_{tot} ($M_\odot$)	t_{late}
B15-1-pw	B15	BSG	1.2	14.2	15.4	156 days
N20-4-cw	N20	BSG	1.4	14.3	15.7	145 days
L15-1-cw	L15	RSG	1.6	13.7	15.3	146 days
W15-2-cw	W15	RSG	1.4	14.0	15.4	148 days
W15-2-cw-IIb	IIb	RSG He core	1.4	3.7	5.1	18 days
16-7b	M15	BSG from merger	1.4	19.5	20.9	1.05 hours

2.2 Centre of Mass per Element

To calculate the centre of mass for the different elements in the SN models I have used the following formula, using a spherical coordinate system. In a system of particles $\boldsymbol{P}_i$, $i = 1, 2, \ldots, n$, with a mass m_i and the coordinates r_i, the centre of mass ***CoM*** is defined as the sum of the weighted average of the position of each particle weighted by the mass of the particle

$$\boldsymbol{CoM} = \frac{m_1 r_1 + m_2 r_2 + \cdots + m_n r_n}{m_1 + m_2 + \cdots + m_n} = \frac{1}{M}\sum_{i=0}^{n} m_i r_i$$

where M is the total mass of the particles in the system (Department of Physics, National Tsing Hua University).

In the models studied in this paper 20 elements are included in the original simulations (Wongwathanarat, 2015). All elements will from this point forward be referred to by their chemical symbol. I have chosen to focus on a number of elements that are important to the SN physics: ^{1}H, ^{4}He, ^{12}C, ^{16}O, ^{28}Si, ^{56}Fe, and ^{56}Ni. Because of ^{56}Ni-decay I also use the combination of ^{56}Ni, ^{56}Co, ^{56}Fe, and the tracer nucleus X, comprised of neutron-rich iron-group elements, in order to clarify and evade eventual uncertainty possible in model M15 (as is discussed in section 5.2). I call the combination of these elements iron-peak elements. The

CoM for the iron-peak elements is calculated as the summation of the CoM for the elements ^{56}Ni, ^{56}Co, ^{56}Fe and the tracer nucleus X, comprised of neutron-rich iron-group elements. As a result of ^{56}Ni-decay, and because the t_{late} of model M15 is only 1.05 hours while the t_{late} of the non-stripped single-progenitor models are more than 100 days, almost all of the original ^{56}Ni remains in model M15 while it has decayed into ^{56}Fe in the non-stripped single-progenitor models. Therefore ^{56}Ni is studied and ^{56}Fe is excluded from model M15, while ^{56}Fe is studied and ^{56}Ni excluded from the non-stripped single progenitor models.

2.3 Density Correlations

I have also used the SN models described earlier to calculate the density for different elements in different layers of the SN ejecta and compare these with each other. The histograms presented in this paper are created using the Python plotting tool Matplotlib.

Because of the effects of ^{56}Ni-decay, ^{56}Ni is studied in model M15, while ^{56}Fe is studied in the non-stripped single progenitor models, as explained in section *2.2*.

3. Results

The results for the previously mentioned SN explosion models are presented below.

3.1 Centre of Mass per Element

The lowest velocity for CoM in all models is that of ^{1}H, while the highest are those of ^{56}Fe, ^{56}Ni, and the iron-peak elements (*Table 2*). The velocity for CoM also seems to decrease with the falling atomic mass in all six models.

Table 2. The centre of mass (CoM) as a velocity for the, in this paper, seven most studied elements (hydrogen, helium, carbon, oxygen, silicon, iron, and nickel, which from this point forward will be referred to according to the notation in the table) in all six models, as well as for the iron-peak elements and the NS.
*The iron-peak elements predominantly have an atomic mass of approximately 56 u.

Element	Atomic Mass [u]	CoM_{B15} [km s^{-1}]	CoM_{N20} [km s^{-1}]	CoM_{L15} [km s^{-1}]	CoM_{W15} [km s^{-1}]	CoM_{IIb} [km s^{-1}]	CoM_{M15} [km s^{-1}]
^{1}H	1.00	9.82	4.56	14.3	21.7	27.4	49.1
^{4}He	4.00	26.6	17.5	37.3	49.8	101	54.6
^{12}C	12.00	51.4	65.4	115	190	389	133
^{16}O	15.99	94.1	98.5	146	312	930	326
^{28}Si	27.98	97.7	103	242	326	1460	552
^{56}Fe	55.93	147	123	396	508	1720	76.9
^{56}Ni	55.94	33.3	84.9	234	329	1720	687
Iron-peak	56*	608	488	1410	1920	6890	1880
NS		106	221	297	486	915	1070

As can be seen in *Figure 3a* the CoM for all elements in the model B15 except for ^{1}H are moving in approximately the same direction. ^{1}H, however, is pictured as moving in the same direction as the neutron star. This phenomenon can also be observed in *Figure 3c*, where the CoM for ^{1}H, as well as that for two other elements with low atomic mass, does not have the same direction as the heavier elements. Note that the NS has a direction opposite that of the entire SN ejecta consisting of the elements in the SN (*Figures 3a-c*).

When the CoM per element is plotted three-dimensionally an interesting fan shape, or co-planar distribution, can be seen. From one angle the CoM for most of the elements have very different directions (left figure in *Figure 3b*), whilst from another angle the CoM lays in the same plane for all elements (right figure in *Figure 3b*). This can also be seen in other models, although the fan shape is much less distinguished there.

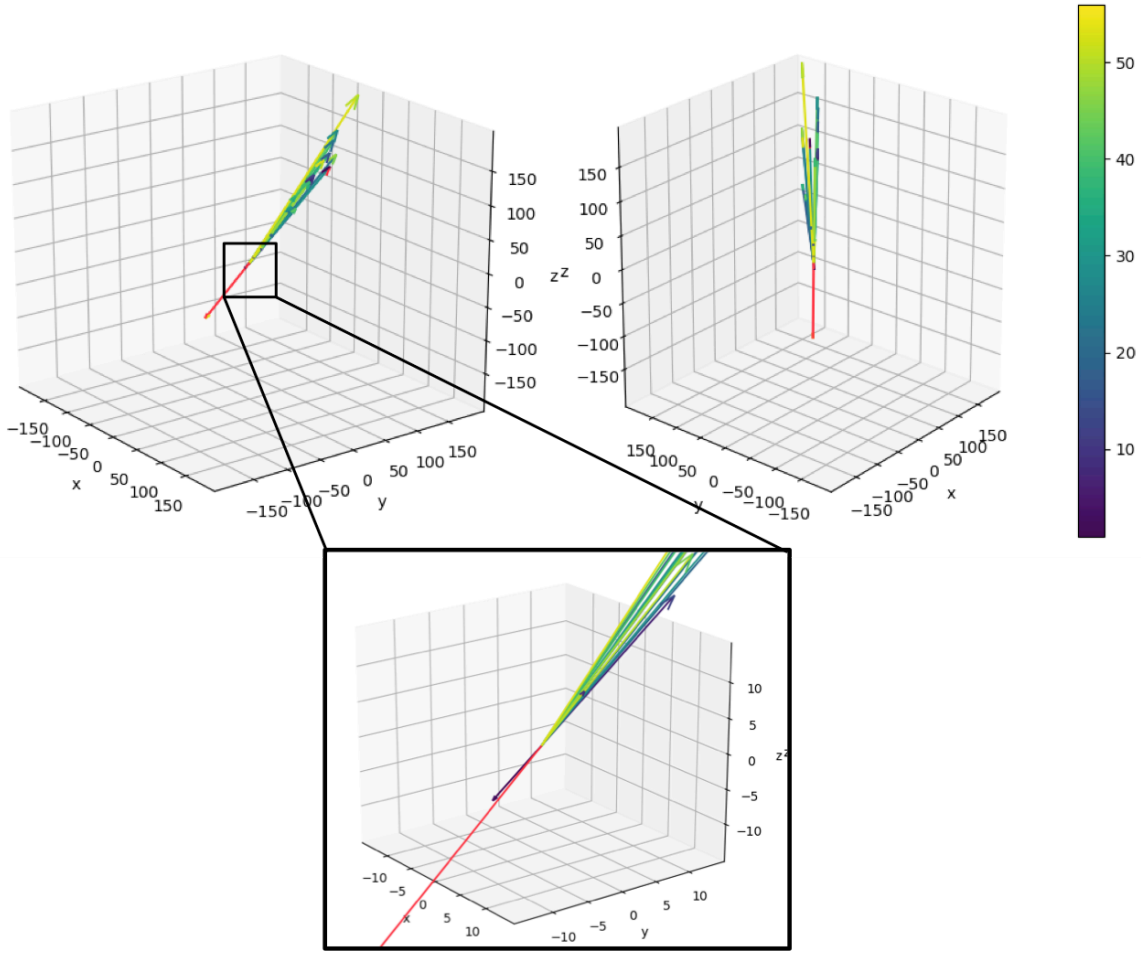

Figure 3a. The CoM [km s^{-1}] for all elements and the NS plotted in 3D for model B15. The colourscheme corresponds to the atomic mass of each element in u (see colourbar). The NS is coloured in orange for visual clarity

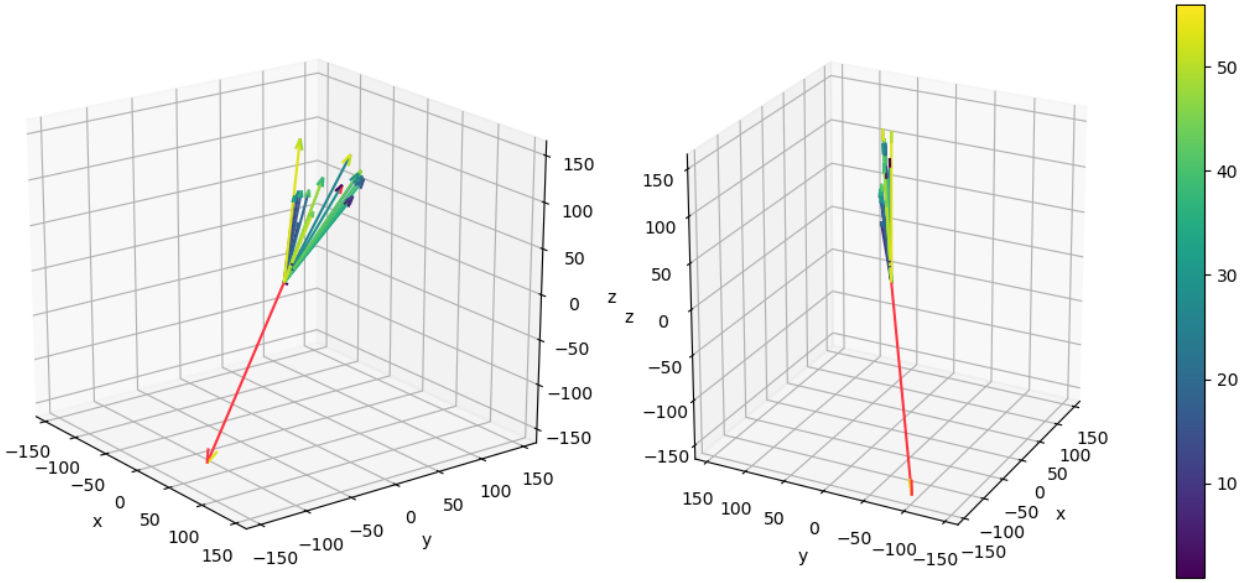

Figure 3b. The CoM [km s^{-1}] for all elements and the NS plotted in 3D for model N20. The colourscheme corresponds to the atomic mass of each element in u (see colourbar). The NS is coloured in orange for visual clarity.

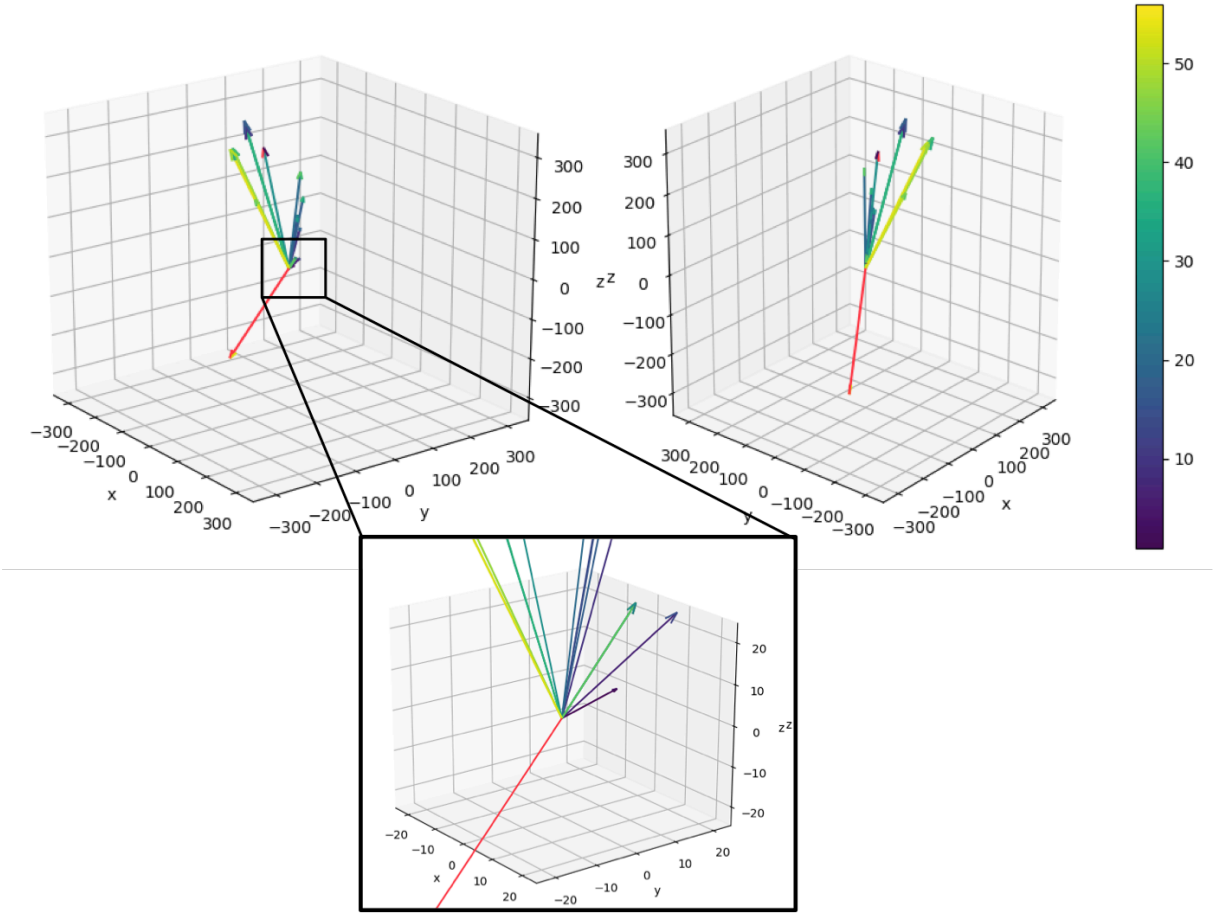

Figure 3c. The CoM [km s^{-1}] for all elements and the NS plotted in 3D for model L15. The colourscheme corresponds to the atomic mass of each element in u (see colourbar). The NS is coloured in orange for visual clarity.

3.2 Density Correlations

I have studied the density of different elements plotted as functions of each other in all six models used in this study. Here, I present the most interesting findings.

The following figures show the density of two elements plotted in the same heat map. The axes show the logarithm of the density at time t_{late} (see *Table 1*). This means that every point on the heat map represents a region with a certain density of element A and a certain density of element B. The brightness of the point then represents how much mass resides in that particular region of the ejecta. For example, *Figure 4* has a bright spot where the density of ^{28}Si is around $10^{-15.6}$ g cm^{-3} , and the density of ^{16}O is around 10^{-13} g cm^{-3}. This means that most of the mass resides in a region with those particular densities of ^{28}Si and ^{16}O.

The elements are more asymmetric when their density ranges over a large interval, and less asymmetric when the interval is smaller.

As can be seen in *Figure 4*, the density of ^{28}Si is high where the density of ^{16}O also is high. *Figure 4* shows a blurry line extending from the bottom left to the top right corner of the figure, which means that, as the density of ^{28}Si increases, so does the density of ^{16}O. This implicates that the two elements are correlated with each other; they can be found in approximately the same locations in the supernova in model B15.

In the innermost layers of the SN in model B15, at t_{late} = 156 days, ^{56}Fe and ^{16}O are anti-correlated; where the density of ^{56}Fe is at its peak the density of the ^{16}O is low and vice versa (*Figure 6*). In the intermediate and outermost layers of the SN ejecta in model B15 ^{56}Fe and ^{16}O are instead correlated, implicating that the majority of regions in the outermost layers contain both ^{56}Fe and ^{16}O (*Figure 6*).

In the inner layers of the SN in model M15, ^{56}Fe and ^{16}O are correlated in a manner similar to the one seen in the outermost layers of the SN in model B15 (*Figure 5* and *6*).

Figure 7 shows ^{56}Ni plotted against ^{16}O in model M15. In the innermost layers of the SN in model M15 the two elements are anti-correlated, in a manner similar to the anti-correlation between ^{56}Fe and ^{16}O in model B15 shown in the top figures of *Figure 6*. In the innermost layers in model M15 ^{56}Ni can be found with densities ranging from $10^{-5.2}$ g s^{-1} to $10^{-3.2}$ g s^{-1}, a range of two orders of magnitude, which implicates that the ^{56}Ni in model M15 is very asymmetric in the innermost layers of the SN (*Figure 7*). ^{16}O on the other hand is less asymmetric in the innermost layers (top figure in *Figure 7*), but very asymmetric in the intermediate regions of the ejecta (bottom figure in *Figure 7*). The range of the density of ^{56}Ni is of approximately 1.5 orders of magnitude in the intermediate regions, indicating that it is slightly less asymmetric there than in the innermost regions (*Figure 7*).

In the intermediate layers in model M15 a gap between two bright spots on the heat map is noted (bottom figure in *Figure 7*). This indicates the occurrence of regions where there is ^{16}O with densities ranging between $10^{-4.6}$ g s^{-1} and $10^{-3.8}$ g s^{-1}, but no ^{56}Ni.

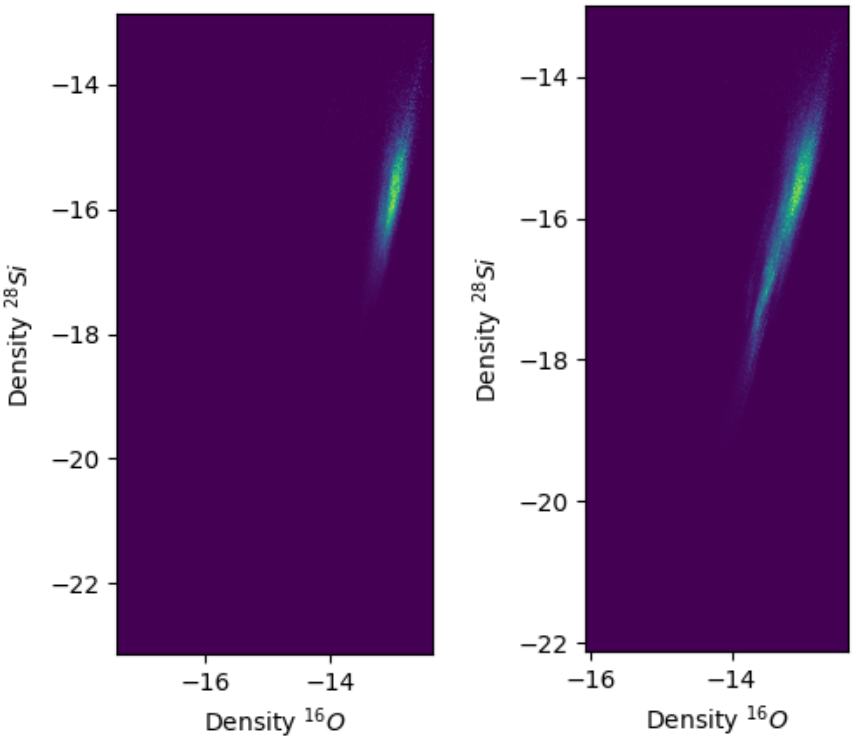

Figure 4. The density of the ^{28}Si in the SN plotted as a function of the density of the ^{16}O in the (Left) innermost 1.84 $M_{\odot}$, and (Right) innermost 12.5 $M_{\odot}$ of the SN. Model: B15, t_{late} = 156 days. The scale is logarithmic showing the exponents on the axes.

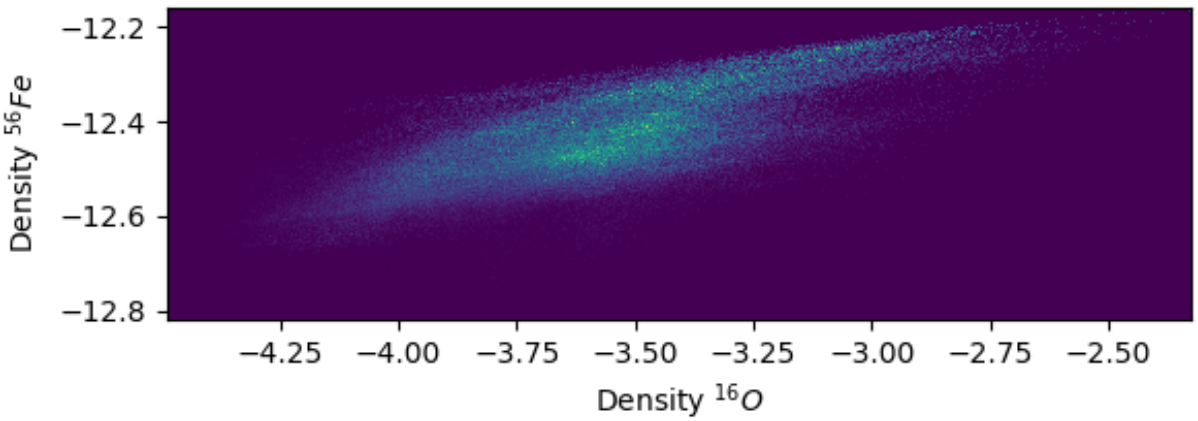

Figure 5. The density of the ^{56}Fe in the SN plotted as a function of the density of the ^{16}O in the innermost 0.10 $M_{\odot}$ of the SN. Model: M15, t_{late} = 1.05 hours. The scale is logarithmic showing the exponents on the axes.

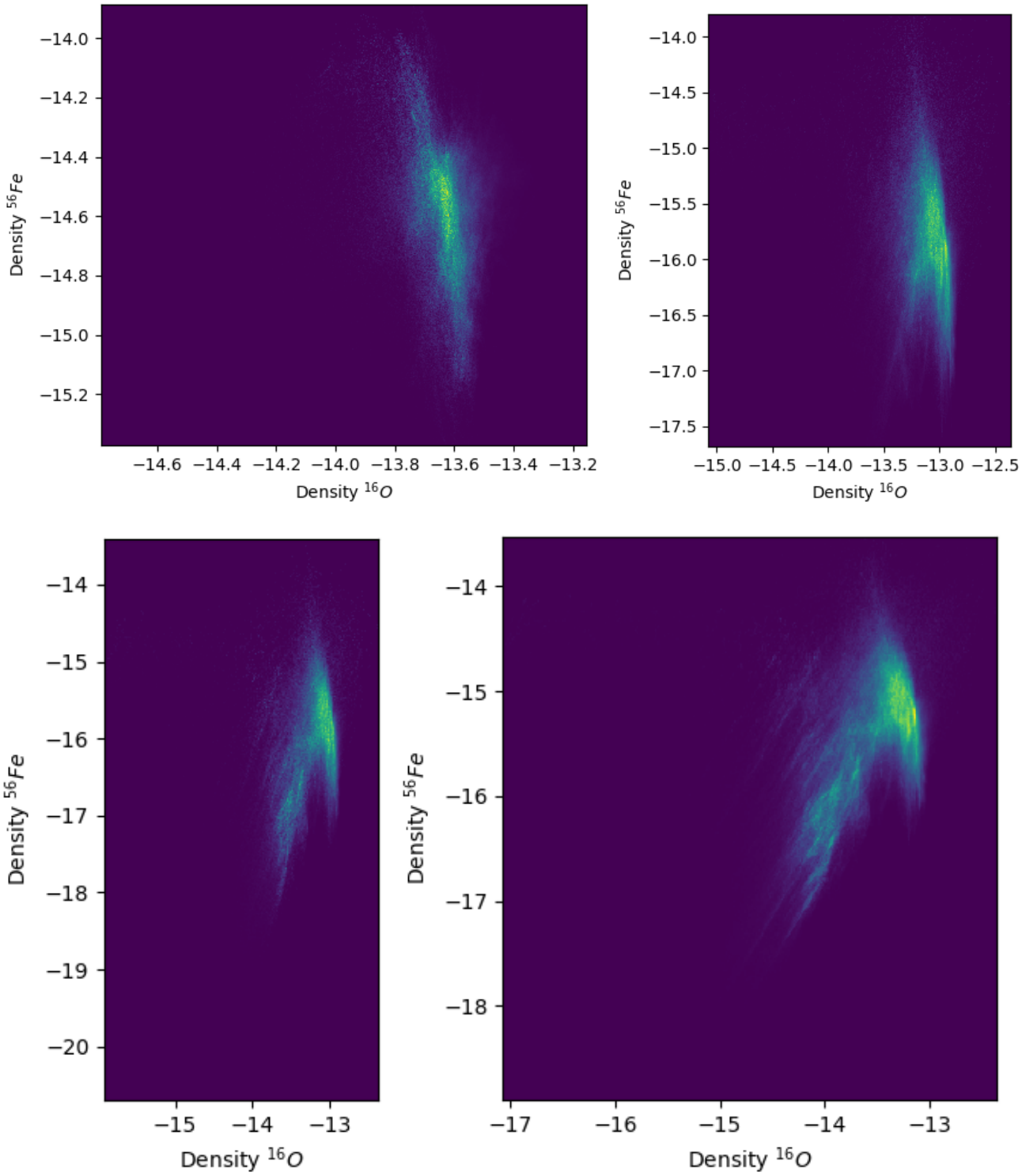

Figure 6. The density of the ^{56}Fe in the SN plotted as a function of the density of the ^{16}O in the (Top left) innermost 0.55 $M_{\odot}$, (Top right) innermost 1.84 $M_{\odot}$, (Bottom left) innermost 5.46 $M_{\odot}$, and (Bottom right) innermost 14.2 $M_{\odot}$ of the SN. Model: B15, t_{late} = 156 days. The scale is logarithmic showing the exponents on the axes.

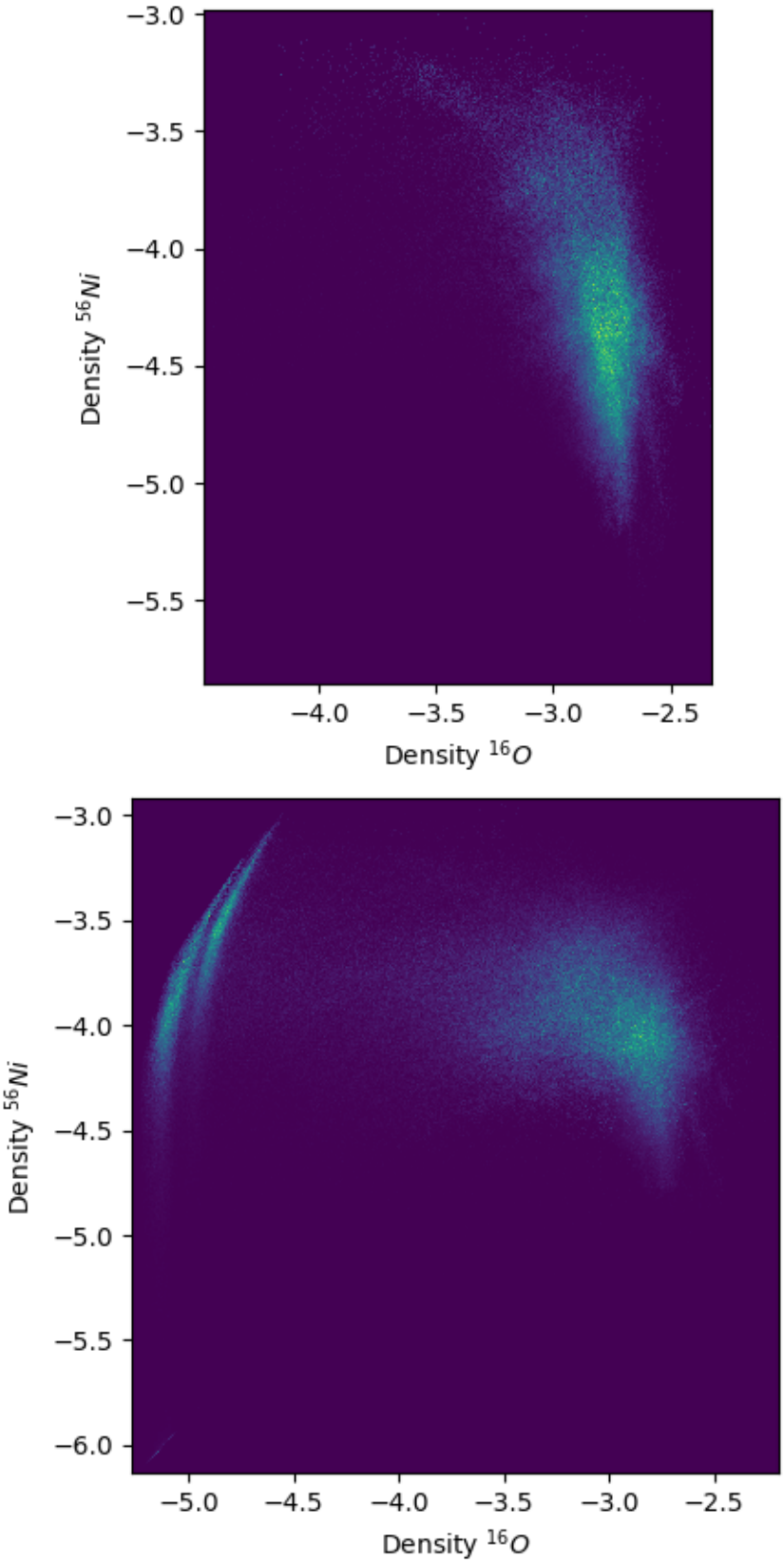

Figure 7. The density of the ^{56}Ni in the SN plotted as a function of the density of the ^{16}O in the (Top) innermost 0.10 $M_{\odot}$, and (Bottom) innermost 1.28 $M_{\odot}$ of the SN. Model: M15, t_{late} = 1.05 hours. The scale is logarithmic showing the exponents on the axes.

4. Discussion

In this study I have received three main results: 1) the elements in the SN seem to be expelled in a co-planar manner; 2) the heaviest elements in the progenitor star are the most asymmetric, and the SN in later stages is more asymmetric in the intermediate than in the inner regions of the SN ejecta; and 3) my results comply with, and strengthen the theory that RT instabilities occur in SNe and partially cause the early asymmetric properties of the elements in the SN. I also propose a novel method of presenting and defining the asymmetries in SNe by using the CoM.

In the three-dimensional plots presented, a co-planar distribution is observed (*Figures 3a-c*). I suggest that this shape may be related to a rotation, or spin, of the SN. In a non-rotating SN the explosion would throw the material in all directions, giving the 3D-figure a more cone-like shape, much like the one seen in model L15 (*Figure 3c*). Because the material seems to be expelled in a single plane in the other models, I suggest that the SN has a rotation causing the material to move in only the equatorial plane. The SN explosion models used in this study are initially non-rotating, meaning that no rotation has been given to the progenitor star. The rotation that my results indicate must therefore be a result of the explosion, or some other mechanism causing the explosion. This is discussed by Wongwathanarat et al. (2013), where it is argued that both theoretical and observational studies expect that a NS, created in a SN explosion, can acquire spin even in simulations with non-rotating progenitor stars. My results suggest that not only the NS, but also the entire SN ejecta, develop spin. The co-planar distribution is the most defined in models N20 and M15, which I theorize to implicate a faster rotation in these two than in the other models. The same reasoning gives model L15 the slowest rotation, because of its more cone-like shape. Assumed that the NS spin is related to the spin of the entire ejecta, my conclusions are supported by results received by Wongwathanarat et al. (2013), which suggest that N20 models generally develop the highest spins. More objective and quantitative measures of the distribution are required for firm conclusions.

In all models the CoM seems to decrease with the falling atomic number, the CoM is the lowest for ^{1}H while it is the highest for the iron-peak elements and ^{56}Fe respective ^{56}Ni. One could speculate that this is a result of the mechanism of the SN explosion. Because the explosion originates from the centre of the progenitor star it affects the elements in the core (i.e. the iron-peak elements) the most, causing them to be the most asymmetric and have the highest velocities. These elements in turn push on the adjacent layers, making them slightly more asymmetric than the outermost layers. This is, of course, only a speculative, but possible explanation. The variations in CoM between elements found in the core of the

progenitor star and the ones found in the intermediate and outer layers could also be a result of RT instabilities causing iron-peak fingers to protrude through the layers of ^{12}C and ^{16}O. This creates plumes of ^{12}C and ^{16}O that fall back towards the core, giving the CoM for the iron-peak elements a higher velocity than that for ^{12}C and ^{16}O (Hammer, 2010). I also found that the iron-peak elements were very asymmetric in the innermost region of the SN in model M15, which had a low t_{late} of only 1.05 hours. This implicates that the elements found in the core of the progenitor, i.e. the iron-peak elements, are very asymmetric from an early stage of the SN explosion. In the inner layers of the SN in model M15, ^{56}Fe and ^{16}O are correlated in a manner similar to the one seen in the intermediate layers of the SN in model B15 (*Figure 5* and *6*). Because model M15 is developed only to a t_{late} = 1.05 hours compared to 156 days in model B15, this might suggest that the asymmetries in the SN are even greater in a later stage of the explosion, and then in the intermediate layers of the SN.

The low CoM for ^{1}H can similarly be explained by the initial position of the ^{1}H-shell; because it is located in the outermost layer of the progenitor star it is not as affected by the shock wave as the core elements and it keeps its nearly spherical shape. This gives it a low velocity for CoM, since the ^{1}H-shell is moving with approximately the same velocity in all directions. This conclusion is supported by discussions of Wongwathanarat et al. (2013), saying that the outgoing explosion shock transfers much of its energy and momentum to the dominating ^{1}H- and ^{4}He-layers in the outer region of the SN, thus making the initially asymmetric explosion more spherical in the outermost layers. The relatively spherical shape of the ^{1}H-shell can also explain why the CoM for ^{1}H has a direction that deviates from the rest of the elements in several of the three-dimensional plots (*Figure 3a-c*). Small irregularities and the overall turbulence in the exploding SN can therefore shift the CoM of ^{1}H and give it a direction opposite the rest of the elements.

My results also comply with, and strengthen the theory that RT instabilities occur in SNe and partially cause the early asymmetric properties of the elements in the SN (Hammer et al. 2010, Sharp 1983, Wollaeger et al. 2017, Wongwathanarat et al. 2015). The anti-correlation between ^{56}Fe and ^{16}O observed in the innermost layers of model B15 might be explained by the RT instabilities that occur in the explosion (*Figure 6*). As described by Hammer et al. (2010), the largest mushroom fingers protruding through the ^{16}O-layer consist mostly of ^{56}Ni that in all non-stripped single progenitor models has decayed into ^{56}Fe, which explains the anti-correlations between the ^{56}Fe and the ^{16}O. The onion structure of the progenitor star is destroyed by the ^{56}Fe-fingers, causing plumes of ^{16}O to fall back towards the centre. The anti-correlation in the densest regions of the SN ejecta observed in *Figure 6* implicate that the densest plumes or mushroom fingers are overabundant of either ^{56}Fe or ^{16}O, which is in agreement with the mechanisms of RT instability in the SN ejecta (Hammer et al. 2010, Sharp 1983, Wongwathanarat et al.

2015). The gap seen in the bottom figure of *Figure 7* could also be evidence of RT instabilities. I interpret the gap between the two bright spots on the heat map as an implication of the occurrence of oxygen plumes in the intermediate layers of the SN with those particular densities containing no ^{56}Ni. The cause of these plumes is most likely the RT instabilities in the SN ejecta. Thus, these findings are also in agreement with the mechanisms of RT instability.

The method of presenting and discussing asymmetries in a SN using the CoM per element is my proposition for future studies in the field. A universal method of presenting and definition of the asymmetries would facilitate comparison of SN explosion models simulated by different research groups using different methods of simulation. One disadvantage regarding this method is that it would be difficult to use as a comparison to observations of real SNe, as the CoM for different elements is very hard to determine from observational data only. Further studies examining geometrical properties that can be deducted from both observational and simulated data are therefore needed to determine if there is one that can be used for this purpose, either on its own or when measured together with the information given by the study of CoM.

This study is based on raw data attained through computer simulations of SN explosions. Because computer simulations and numerical models are created in a perfect environment, they can never match reality down to every single detail. They are therefore used as a complement rather than as a replacement for observational studies. Since I have not had access to observational data during my studies, I have only been able to use computer simulations. The method in this study could thus be improved through comparison of the received results with observations of real SNe, in order to determine if they truly correspond. This could be an interesting study for the future.

A possible source of error in this study is the low t_{late} of model M15. The t_{late} for model M15 is as low as 1.05 hours, far lower than that for the remaining models. As explained in sections *1.3*, *4.1*, and *4.3*, this results in very little ^{56}Ni having decayed into ^{56}Fe. The low mass of ^{56}Fe could increase the uncertainty for that particular set of data, making the results concerning the ^{56}Fe in model M15 more uncertain than the other results. To avoid this source of error no results are based solely on the ^{56}Fe in model M15, but ^{56}Ni has been used instead. The results achieved also correspond with existing theory, making them probable.

This project has generated many propositions for further studies. In order to further clarify the composition of elements and their geometrical properties in SNe future studies are needed. These could include studies of the dispersion of elements in different layers of the SN ejecta, in order to show in what

radii interval the different elements occur. Repeating the studies of density correlation presented in this paper for an extended amount of elements would also be of significance. It would also be interesting to repeat these studies for all different SN explosion models currently in use. This would allow comparisons of the asymmetries in different models, to see if all groups studying SN models would receive similar results. Comparing these results with the CoM calculated from observational data would, although challenging, also be very interesting. Furthermore, an extended study of geometrical properties in observational data would be of interest. Finally, further studies are needed to determine the exact reason for the variances in asymmetry between the different elements.

5. Conclusions

SN explosions are among the most energetic phenomena in the universe, as they supply the universe with chemical elements, kinetic energy, and trigger the formation of stars. This makes understanding the cause and inner processes of SNe very interesting to astrophysicists. The asymmetric properties in SNe are thought to play a crucial role in the origin and mechanisms of the SN explosion. In study of these asymmetries, and other physical attributes of the SN, numerical simulations are used in addition to observational data. Studies of these simulation models provide information and insights into the SN mechanisms that cannot be obtained solely through observations.

In this project I have used the programming language Python to study six of these SN models created and described by Wongwathanarat et al. (2015) and Menon et al. (2019). I have quantified geometrical properties such as the CoM and the density of the different elements in the SN ejecta. I have identified a tentative co-planar distribution of the CoM for the elements; further studies are needed to firmly conclude if the distributions are results of a rotation in the SN. My results suggest that the heavier elements in the SN are the most asymmetric and that their CoM have the highest velocities. My study of the density correlations show that the iron-peak elements are extremely asymmetric from very early on and that they, in the later stages, are more asymmetric in the intermediate layers than in the innermost layers. My results also correspond with previous theory regarding the RT instabilities in SNe. Finally, I propose a method of defining asymmetries by the CoM for the elements in the ejecta.

Acknowledgements

I would like to give special thanks to my main supervisor Dennis Alp for his valuable and constructive suggestions during this project. I would also like to thank Blackebergs gymnasium, the Royal Institute of Technology (KTH), and the Core-Collapse Supernova group at Max-Planck Institute for Astrophysics for providing the essential data for this project. Finally, I would like to acknowledge the support and advice provided by Alexander Hedlund, and my family.

6. References

1. Alp, D., Larsson, J., Fransson, C., Gabler, M., Wongwathanarat, A., & Janka, H.-T. 2018, The Astrophysical Journal, 864, 175
2. Filippenko, Alexei V., Kleiser, Io K. W., Silverman, Jeffrey M., Ganeshalingam, Mohan, Li, Weidong, Poznanski, Dovi, …, Matheson, Thomas. 2011, Monthly Notices of the Royal Astronomical Society, 415, 372
3. Hammer, N. J., Janka, H. T., & Müller, E. 2010, The Astrophysical Journal, 714, 1371
4. Menon, A., Heger, A., & Utrobin, V. 2019, Monthly Notices of the Royal Astronomical Society, 482, 438
5. Nadyozhin, D. K. 1994, The Astrophysical Journal, 92, 527
6. Wollaeger, R. T., Hungerford, A. L., Fryer, C. L., Wollaber, A. B., Rossum, D. R. v., & Even, W. 2017, The Astrophysical Journal, 845, 168
7. Wongwathanarat, A., Janka, H. T., & Müller, E. 2013, Astronomy & Astrophysics, 552, A126
8. Wongwathanarat, A., Müller, E., & Janka, H. T. 2015, Astronomy & Astrophysics
9. Clark, S. (1997). Universe in Focus. The Story of the Hubble Telescope. Singapore: Barnes & Noble Books.
10. NASA. (Last updated December 8th 2018). NASA Science. Retrieved from https://science.nasa.gov/astrophysics/focus-areas/how-do-stars-form-and-evolve on December 9th 2018
11. NE. (1996). *Nationalencyklopedin* (Vol. XIX). (C. Engström, Red.) Höganäs: Bokförlaget Bra Böcker AB.
12. Smithsonian Astrophysical Observatory. (May 6th 2013). Chandra X-ray Observatory. Retrieved from Supernovas & Supernova remnants: http://chandra.harvard.edu/xray_sources/supernovas.html on December 27th 2018

13. Smithsonian Astrophysical Observatory. (April 3rd 2017). Chandra X-ray Observatory. Retrieved from http://chandra.harvard.edu/ on December 25th 2018
14. Smithsonian Astrophysical Observatory. (August 2nd 2017). Chandra X-ray Observatory. Retrieved from http://chandra.harvard.edu/edu/formal/stellar_ev/story.html on September 25th 2018
15. Taylor Redd, N. (Februari 23rd 2018). Main Sequence Stars: Definition & Life cycle. Retrieved from https://www.space.com/22437-main-sequence-stars.html on December 9th 2018
16. Wikipedia. (December 22nd 2018). Sun. Retrieved from https://en.wikipedia.org/wiki/Sun on December 27th 2018
17. Wikipedia. (September 27th 2018). Type II Supernova. Retrieved from https://en.wikipedia.org/wiki/Type_II_supernova#Type_IIb_supernovae on December 29th 2018

7. Appendix

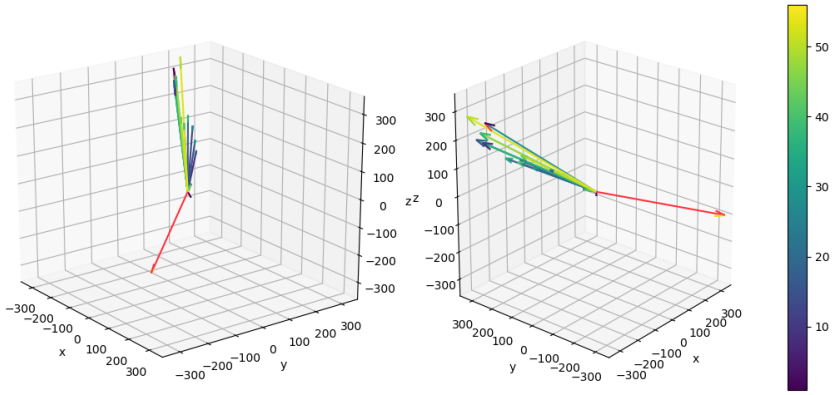

Appendix 1. The CoM [km s^{-1}] for all elements and the NS plotted in 3D for model W15. The colourscheme corresponds to the atomic mass of each element in u (see colourbar). The NS is coloured in orange for visual clarity.

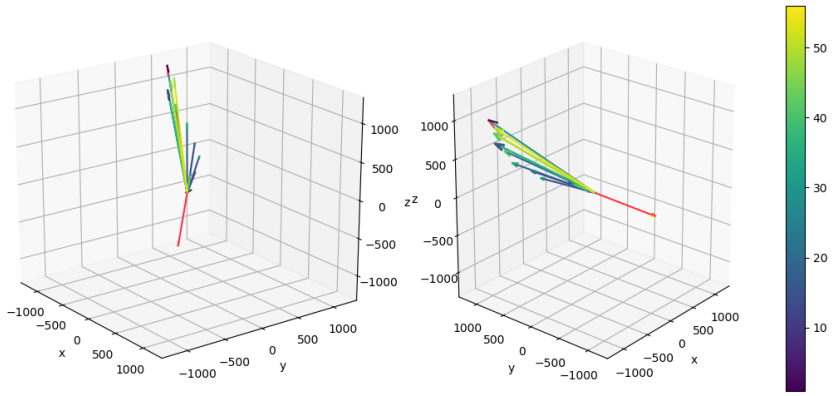

Appendix 2. The CoM [km s^{-1}] for all elements and the NS plotted in 3D for model IIb. The colourscheme corresponds to the atomic mass of each element in u (see colourbar). The NS is coloured in orange for visual clarity.

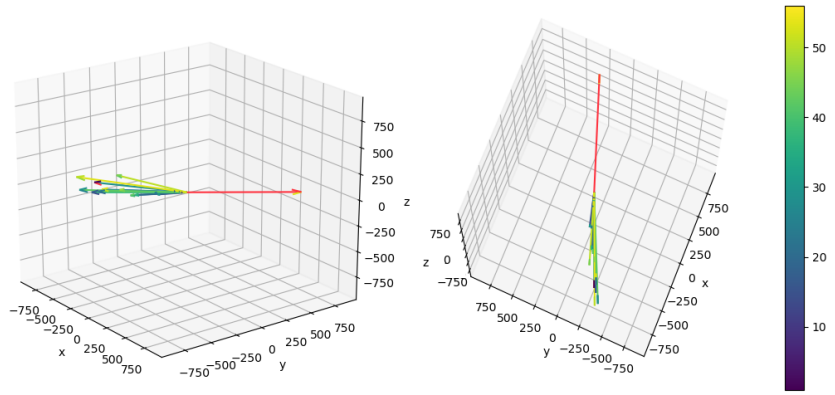

Appendix 3. The CoM [km s^{-1}] for all elements and the NS plotted in 3D for model M15. The colourscheme corresponds to the atomic mass of each element in u (see colourbar). The NS is coloured in orange for visual clarity.